Metallization in hydrogen-helium mixtures

Winfried Lorenzen,[1] Bastian Holst,[1,2] and Ronald Redmer[1]

[1]*Institut für Physik, Universität Rostock, D-18051 Rostock, Germany*
[2]*CEA, DAM, DIF, F-91297 Arpajon, France*
(Received 2 September 2011; revised manuscript received 14 October 2011; published 1 December 2011)

Hydrogen-helium mixtures have long been predicted to undergo demixing at high pressures of several megabars which occur in the interiors of giant planets such as Jupiter and Saturn. This effect is most important to understand their evolution and current interior structure. *Ab initio* calculations have already proven their potential to give precise predictions for the demixing line for pressures above 4 Mbar, well above a first-order phase transition from molecular to metallic hydrogen. Here we calculate the miscibility gap for lower pressures between 1 and 2 Mbar using *ab initio* molecular dynamics simulations. By using the Kubo-Greenwood formula we obtain the electrical conductivity and reveal the close connection between metallization in the hydrogen subsystem and the location of the miscibility gap. Especially, we find direct evidence for H-He demixing by performing simulations for large particle numbers.

I. INTRODUCTION

The behavior of hydrogen, helium, and their mixtures at high pressures of several megabars is very important for understanding the interior of giant planets.[1–3] Demixing of hydrogen and helium at these conditions was proposed as an explanation for the lower helium content in the atmosphere of Jupiter and Saturn compared to the solar value and the observed excess luminosity of Saturn. It was already shown[4,5] that this effect has the potential to yield the correct age of Saturn by evaluating inhomogeneous evolution models and assuming a modified H-He equation of state (EOS).

To the best of our knowledge, few experimental data exist for the high-pressure phase diagram of H-He mixtures,[6–8] so far up to ∼0.3 Mbar and 7000 K, i.e., not yet reaching the conditions inside giant planets. Conductivity measurements in H-He mixtures up to Mbar pressures were reported by Ternovoi *et al.*[9]

Various attempts to calculate the miscibility gap in the H-He system have been performed in the past.[10–16] With the advancement of computational power, this problem was tackled with *ab initio* methods.[17,18] In particular, Klepeis *et al.*[19] used the local density approximation within density functional theory (LDA-DFT) for solid hydrogen-helium alloys. Later this approach was refined by Pfaffenzeller *et al.*[20] by using Car-Parrinello molecular dynamics (CP-MD) simulations for the liquid, combining (classical) molecular dynamics simulations for the ions with LDA-DFT for the electrons. However, the critical temperatures derived from these two studies differed by large amounts, predicting complete demixing in Jupiter and Saturn in the first case and no demixing in the second case.

This discrepancy was resolved recently by performing consistent finite-temperature DFT-MD simulations[21,22] within the generalized gradient approximation (GGA), showing conclusive evidence for hydrogen-helium demixing at conditions relevant for Jupiter and especially Saturn. While Morales *et al.*[21] could circumvent approximations for the entropy of mixing by using thermodynamic integration, Lorenzen *et al.*[22] could calculate a more extensive data set within the approximation of ideal entropy of mixing. The results of

both approaches are in good agreement, indicating a small influence of nonideal entropy contributions (at least for the low He concentration relevant for Jupiter and Saturn) and the importance of an accurate data set for the derivation of the miscibility gap from the Gibbs free energy.

Both hydrogen and helium are expected to undergo a metal-to-nonmetal transition at conditions found in the interior of giant planets. Applying DFT-MD simulations, Lorenzen *et al.*[22] found strong evidence that metallization in the hydrogen subsystem is the driving force of demixing. Consequences of the nonmetal-to-metal transition in hydrogen have been discussed for decades. Most important questions in this context are whether or not metallization is accompanied by a first-order phase transition, as suggested already by Landau and Zeldovich,[23] and where the critical point of this transition is located in the phase diagram. While the transition to liquid metallic hydrogen has been found experimentally,[24,25] to the best of our knowledge, no clear evidence for a first-order phase transition has been observed so far. Quasi-isentropes derived from shock-compression experiments[26] may show a signature of that transition.

Most chemical models predict a pronounced first-order phase transition with a critical temperature located at ∼15 000 K.[16,27–31] Accurate EOS data gained from *ab initio* DFT-MD simulations indicate a first-order phase transition in the liquid with a critical temperature of less than 2000 K.[32,33] Although an experimental verification of this liquid-liquid phase transition is still missing, these results are more reliable because the assumptions of chemical models (e.g., well-defined bound states such as atoms and molecules, effective two-particle potentials between them, the use of perturbation theory) are avoided in this strongly correlated quantum regime.

In this paper we extend our previous calculations of the miscibility gap[22] to lower pressures between 1 and 2 Mbar, i.e., conditions close to the liquid-liquid phase transition in hydrogen as mentioned above. In particular, we study the metallization in hydrogen-helium mixtures with different helium fractions $x = N_{He}/(N_{He} + N_H)$ and prove the close connection between the metallization of hydrogen and the demixing of helium. Especially, we see direct evidence for

H-He demixing by performing simulations with particle numbers as large as computationally tractable today.

In Sec. II we describe the method of DFT-MD simulations. Section III deals with the calculation and discussion of the electrical conductivity as a direct signature of metallization, while in Sec. IV we present results for the miscibility gap. In Sec. V we show and discuss results of very involved calculations for hydrogen-helium mixtures with large particle numbers, showing demixing directly in the simulation box. Conclusions are given in Sec. VI.

II. DFT-MD SIMULATIONS

We perform *ab initio* simulations with the code VASP,[34–36] which combines a quantum mechanical treatment of the electrons using finite temperature density functional theory[37–39] with a classical molecular dynamics simulation for the ions—see, e.g., Refs. 22, 33, and 40–42.

We use the projector augmented-wave method,[43,44] together with an energy cutoff of 1200 eV for the expansion of the electron wave functions in plane waves. For the crucial electronic exchange-correlation functional we employ the GGA in the parametrization of Perdew, Burke, and Ernzerhof (PBE).[45] The Brillouin zone was sampled at the Baldereschi mean value point,[46] which showed best agreement with a sampling using a higher number of **k** points—see also Ref. 33.

The MD simulations were performed for 32–1536 atoms (64–2048 electrons) in a supercell with periodic boundary conditions. The temperature of the ions was controlled by a Nosé thermostat.[47] By choosing the size of the simulation box, the density of the system is fixed. After reaching thermodynamic equilibrium the system was further simulated for several thousand time steps of 0.4 fs to obtain the EOS data.

We have done extensive convergence tests with respect to particle number, **k**-point sampling, energy cutoff, and the size of the time step, ensuring a convergence with results of better than 1%.

III. ELECTRICAL CONDUCTIVITY

The dynamic conductivity $\sigma(\omega)$ is derived from the Kubo-Greenwood formula[48–52]

$$
\sigma(\omega) = \frac{2\pi e^2}{3 V m_e^2 \omega} \sum_{\mathbf{k}} w_{\mathbf{k}} \sum_{j=1}^{N_b} \sum_{i=1}^{N_b} [f_{j,\mathbf{k}} - f_{i,\mathbf{k}}]
$$
$$
\times |\langle \Psi_{j,\mathbf{k}} | \hat{\mathbf{p}} | \Psi_{i,\mathbf{k}} \rangle|^2 \delta(E_{i,\mathbf{k}} - E_{j,\mathbf{k}} - \hbar\omega), \quad (1)
$$

where e is the electron charge, m_e the mass of the electron, V the volume of the simulation box, and ω the frequency. The summation over the matrix elements of the Bloch functions with the momentum operator $\hat{\mathbf{p}}$, weighted with the difference of the Fermi occupations $f_{i,\mathbf{k}}$, is performed over all N_b bands. This formula is evaluated for snapshots of equilibrated simulations with 256 electrons (128–256 atoms). For these calculations we use a $4 \times 4 \times 4$ Monkhorst-Pack[53] grid to reach a convergence of better than 5% accuracy for most of the snapshots. However, especially in the nonmetallic region, reaching good convergence is more demanding, but always better than the variation between different snapshots. The dc
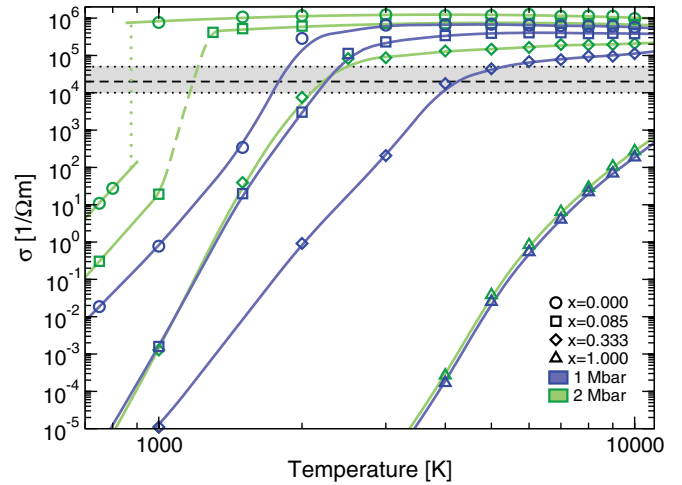

FIG. 1. (Color) Electrical conductivity for different helium fractions x at 1 Mbar (blue) and 2 Mbar (green). The lines are a guide to the eye. The gray area around the Mott minimum metallic conductivity of $2 \times 10^4 / \Omega$ m (black dashed line) is used to determine the temperature of metallization.

electrical conductivity is taken as the static limit of the dynamic conductivity.

Since it is not possible to perform constant pressure MD simulations with VASP, we used the following scheme to get the electrical conductivity at a given pressure P: First we performed two MD simulations with resulting pressures P_1 and P_2 near P, i.e., $0.98 \times P < P_1 < P < P_2 < 1.02 \times P$. From these simulations we extracted 20–40 snapshots, calculated their electrical conductivity and their pressure, and interpolated the results to the given pressure P.

In Fig. 1 we show the resulting conductivities of various hydrogen-helium mixtures as functions of the temperature at constant pressures of 1 and 2 Mbar. Since there is no well-defined criterion for a minimum metallic conductivity at finite temperatures, we use values between $1 \times 10^4 / \Omega$ m and $5 \times 10^4 / \Omega$ m (gray area), motivated by the value of $2 \times 10^4 / \Omega$ m derived by Mott at $T = 0$ K (dashed black line), to distinguish between the *metallic* and *nonmetallic* behavior of the mixture. A more detailed discussion of metal-nonmetal transitions at finite temperatures can be found in Ref. 54.

In the nonmetallic region (below the gray area) the conductivity rises dramatically with temperature (over many orders of magnitude within a few thousand Kelvin) for all considered mixtures and pressures. At 1 Mbar the transition to metallic-like conductivities is always continuous, since these states are above the critical point of the first-order liquid-liquid phase transition in hydrogen.[32,33] However, this is not the case for 2 Mbar, where a first-order transition occurs in pure hydrogen ($x = 0$). This can be identified by the jump from $1 \times 10^2 / \Omega$ m to nearly $1 \times 10^6 / \Omega$ m at $T \approx 875$ K (dotted line). So far it is not clear if a first-order liquid-liquid phase transition exists in hydrogen-helium mixtures, therefore, we have plotted the transition from nonmetallic to metallic conductivities at $x = 0.085$ with a dashed line.

The addition of helium generally lowers the conductivity since it is nonmetallic under these conditions.[55–57] At the highest temperatures considered here the conductivity reaches
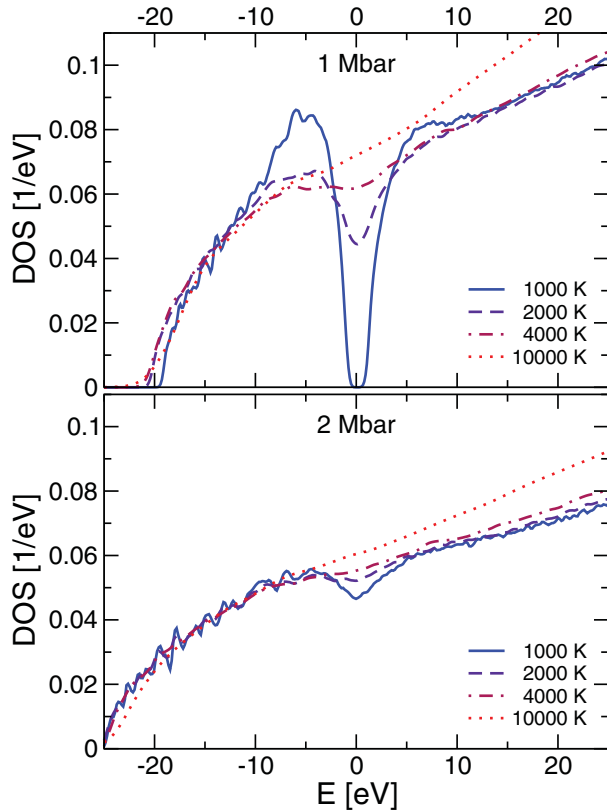
FIG. 2. (Color online) Density of states for hydrogen at $P = 1$ Mbar (top) and $P = 2$ Mbar (bottom) for several temperatures between 1000 and 10 000 K. The energies are shifted such that the Fermi energies are at zero.

FIG. 3. (Color online) Density of states for helium at $P = 1$ Mbar (top) and $P = 2$ Mbar (bottom) for several temperatures between 4000 and 10 000 K. The energies are shifted such that the Fermi energies are at zero.

values above $1 \times 10^2 / \Omega$ m, still well in the nonmetallic region. Additionally, the increase in conductivity gets less steep with more helium in the system, which can be explained by the different metallization mechanisms for hydrogen and helium. This is illustrated via the density of states (DOS) shown in Figs. 2 and 3.

At 1 Mbar hydrogen has still a small band gap at 1000 K, which is already closed at 2000 K, and vanishes completely at 10 000 K. At 2 Mbar the behavior is similar, however, due to the increased density, the band gap is already closed at 1000 K. Therefore, the main metallization mechanism in hydrogen is the closure of the band gap or the overlap of valence and conduction bands, respectively. This leads to drastic increases in the electrical conductivity in a very small temperature range. All these results are in good agreement with previous calculations for the metallization transition in hydrogen[32,33,41] and its phase diagram.[32,33,42,58]

The behavior of helium is completely different. A very pronounced band gap exists at all conditions considered. The only contribution to the conductivity stems from the finite occupation of the conduction band at high temperatures. Therefore, the conductivity increases with temperature also for helium, although much slower than in hydrogen. This behavior agrees with previous results.[55–57]

Note that the values for the band gap and the conditions for its closure depend on the exchange-correlation functional used in the DFT calculations and also on the exact method to identify
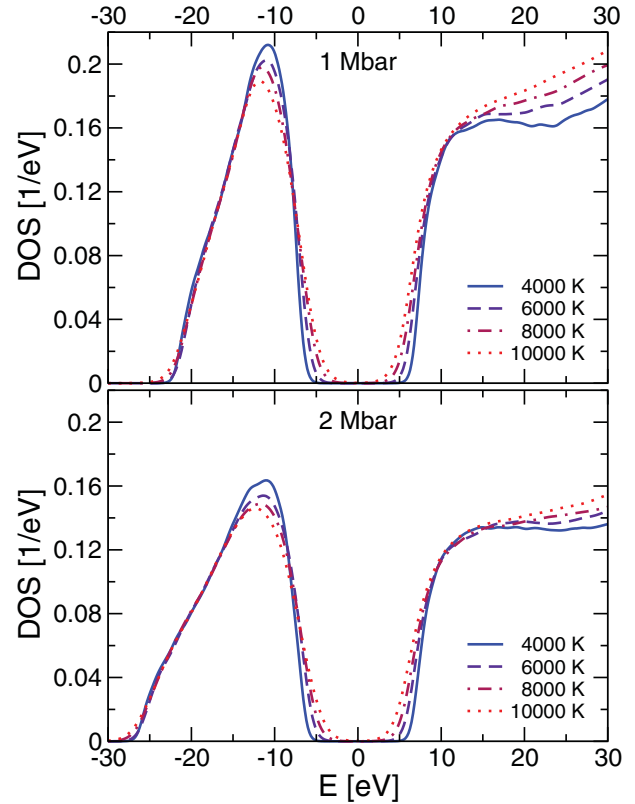
the width of the band gap at finite temperatures. The former uncertainties can be resolved by using exact exchange[59] or hybrid functionals[60,61] in the DFT schema, by performing GW calculations,[62] or within quantum Monte Carlo techniques.[63,64] However, implementing these methods into MD simulations is still computationally very expensive. Since the used PBE functional is known to underestimate the band gaps, we expect that the metallization temperatures would be increased by a more advanced method. Special attention has to be paid to the latter uncertainties when comparing different results.

IV. MISCIBILITY GAP

To study the impact of the metallization on demixing we have extended our previous calculations of the miscibility gap[22] to lower pressures of 1 and 2 Mbar. It is derived from the Gibbs free energy of mixing

$$\Delta G(x) = G(x) - x G(1) - (1-x) G(0) \qquad (2)$$
$$= \Delta U(x) + P \Delta V(x) - T \Delta S(x), \qquad (3)$$

where U is the internal energy, V the volume, T the temperature, and S the entropy. $\Delta U(x)$, $\Delta V(x)$, and $\Delta S(x)$ are defined analogously to Eq. (2). Since the entropy of mixing is not directly accessible to the simulations, we used the ideal entropy of mixing

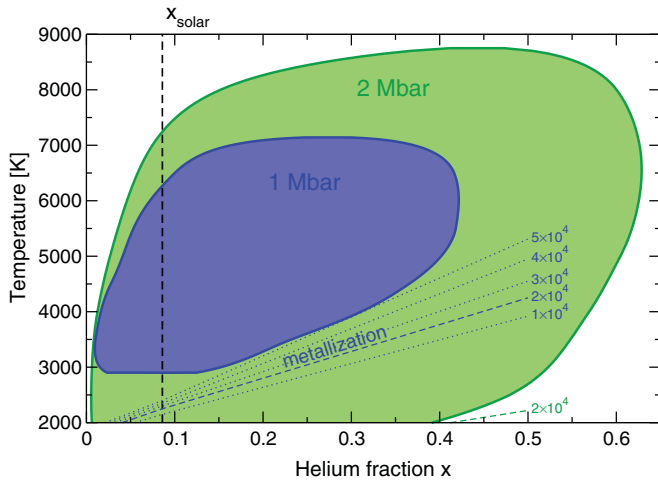$$T \Delta S(x) = -k_B T (x \ln(x) - (1-x) \ln(1-x)). \qquad (4)$$

FIG. 4. (Color online) Miscibility gap in the hydrogen-helium system for 1 Mbar (blue/dark gray) and 2 Mbar (green/gray). Also shown are isolines of the electrical conductivity near the Mott value of $2 \times 10^4/\Omega$ m (dashed and dotted lines). The mean solar helium fraction of $x_{\mathrm{solar}} = 0.086$ as relevant for Jupiter and Saturn is indicated.
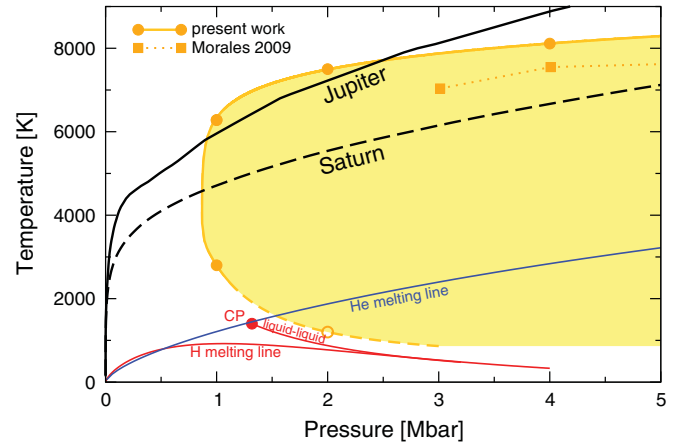

FIG. 5. (Color online) Demixing region (yellow/light gray area) for a helium fraction of $x = 0.086$ in comparison with the isentropes (black) of Jupiter (Ref. [2]) (solid line) and Saturn (dashed line). The filled circles are the calculated data from Fig. [4] and Ref. [22], and the open circle at 2 Mbar is extracted from the conductivity data in Fig. [1]. The line is a fit to these points. The results of Morales *et al.* (Ref. [21]) for the demixing line are also shown (squares). We compare with the phase diagram of hydrogen (red/medium gray). The melting line is taken from Ref. [32] and the coexistence line of the liquid-liquid phase transition with its critical point from Ref. [33]. For helium we show the melting line [blue/dark gray; Kechin-type fit (Ref. [65]) to experimental data (Refs. [66–70]) and our recent high-pressure prediction (Ref. [22])].

These calculations were performed with 32–64 atoms (64 electrons) as in Ref. [22]. For each considered pressure and temperature the Gibbs free energy of mixing is analyzed with a double tangent construction to get the region of demixing—for details see Ref. [22].

Morales *et al.*[21] applied thermodynamic integration in order to calculate the entropy of mixing. For this procedure additional EOS data at each helium fraction is needed for the integration to be accurate. However, for this study we decided to apply the ideal approximation for the entropy of mixing in favor of the number of considered helium fractions. As a consequence, we were able to analyze up to 33 different helium fractions in order to apply the double tangent construction very accurately. Comparison shows that the demixing curves derived from both approaches are very similar. Taking into account the current development of computing power, it will be possible to combine the exact calculation of the Gibbs free energy with a highly accurate double tangent construction in the future.

The resulting miscibility gap is shown in Fig. [4]. We have also extracted the temperature of metallization from Fig. [1] using different values for the conductivity as a criterion, including the minimum metallic conductivity of $2 \times 10^4/\Omega$ m as proposed by Mott for $T = 0$ K. Although it is not possible to distinguish sharply between *metallic* and *nonmetallic* states at finite temperatures, the isolines of the electrical conductivity clearly show a close connection between metallization and demixing. Most strikingly, the beginning of the demixing islands at 1 and 2 Mbar coincides very well with the respective metallization temperatures. However, for 2 Mbar metallization occurs already at much lower temperatures, e.g., below 1000 K for pure hydrogen,[33] merging the demixing region with the area of possible solid hydrogen-helium alloys. A detailed study of such alloys would be an enormous effort by itself and is not within the scope of this paper, especially since these states are

not relevant for the interior of solar giant planets. Therefore, we only show the miscibility gap down to 2000 K, i.e., above the melting temperature of helium.[22]

As in Refs. [21],[22], we show the demixing line for the mean helium fraction in Jupiter and Saturn in Fig. [5], however, this time for the lower pressures considered here. While the agreement with the calculations of Morales *et al.*[21] is good (taking into account all uncertainties in both methods), their deviations and the closeness of the demixing temperature to the temperature along the Jovian isentrope show the necessity to have still more accurate data in the low-pressure region in order to make a definite statement regarding demixing in Jupiter. The temperature inside Saturn is lower than in Jupiter so that its isentrope is deep inside the demixing region for both calculations. Thus, demixing is very important for the interior of giant planets, more so for Saturn than for Jupiter.

The islands of demixing in Fig. [4] lead to a demixing region with lower and upper limits in Fig. [5]. This is a direct consequence of the metallization as the driving force of demixing, since the lower boundary is determined by the metallization of hydrogen. This is nicely illustrated by the coexistence line of the nonmetal-to-metal phase transition[22] in Fig. [5]. Our calculations show also that the prediction of classical Monte Carlo simulations[71] for 1500 K and 0.45 Mbar, which was included in our previous paper,[22] is no longer valid there. The melting lines of hydrogen and helium indicate the merging of possible hydrogen-helium alloys and the demixing region, but also their unimportance for most planetary interiors.
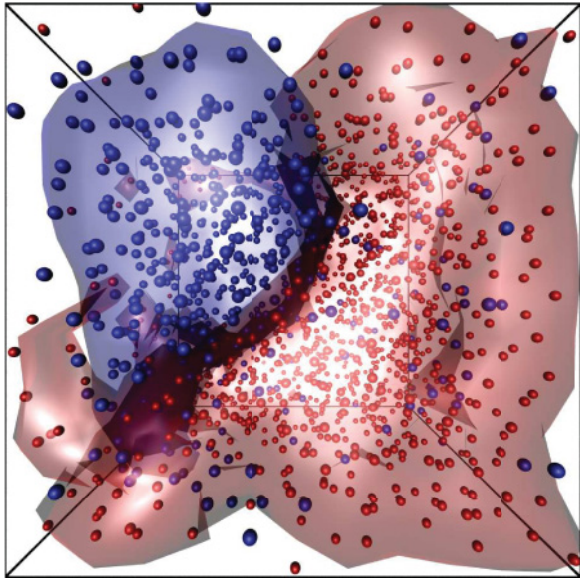
FIG. 6. (Color) Snapshot of a simulation for $x = 1/3$, $\varrho = 4$ g/cm^3, $T = 6000$ K, and $P \approx 20$ Mbar visualized with the VMD program (Ref. 72). Shown are the ions (small spheres) and isosurfaces of the specific particle density for $n_i = 0.5/$Å^3. Blue: helium; red: hydrogen.

V. DIRECT SIMULATION OF DEMIXING

To study the effect of demixing directly, i.e., without using the ideal entropy of mixing or thermodynamic integration, we have performed simulations with 2048 electrons for $x = 1/3$, i.e., 1024 hydrogen atoms and 512 helium atoms, at a constant density of $\varrho = 4$ g/cm^3 and temperatures between 6000 and 12 000 K. With this high (and demanding) particle number it was possible to see demixing effects directly inside the simulation box. A typical snapshot of such a simulation at 6000 K, i.e., inside the demixing region, is shown in Fig. 6. We can identify helium-rich (blue) and helium-poor (red) regions. Note that we did not prepare a demixed state but started from a homogeneously mixed one and then let the system equilibrate. After a simulation time of ~1 ps (a few thousand time steps) the demixing could be seen clearly and was stable until the end of the simulation (a further 3-ps simulation time). At higher temperatures the demixing effect decreases.

For a more quantitative evaluation we have calculated the radial distribution functions from these simulations—see Fig. 7. Inside the demixing region, due to the formation of helium or hydrogen droplets, the probability of finding an ion of the same species in the vicinity of an ion is enhanced compared to an even distribution of ions. This results in an increased radial distribution function at low distances for H-H and He-He, while the H-He distribution function is decreased at low distances.

To further analyze the droplet formation we have determined the center of mass of the helium droplet at each time step of the simulation and evaluated the helium fractions inside spherical shells around this center of mass. This is shown for the same conditions as before in Fig. 8. For 6000 K, i.e., well inside the demixing region, a very pronounced helium droplet with a helium fraction of approximately $x = 0.98$ appears.
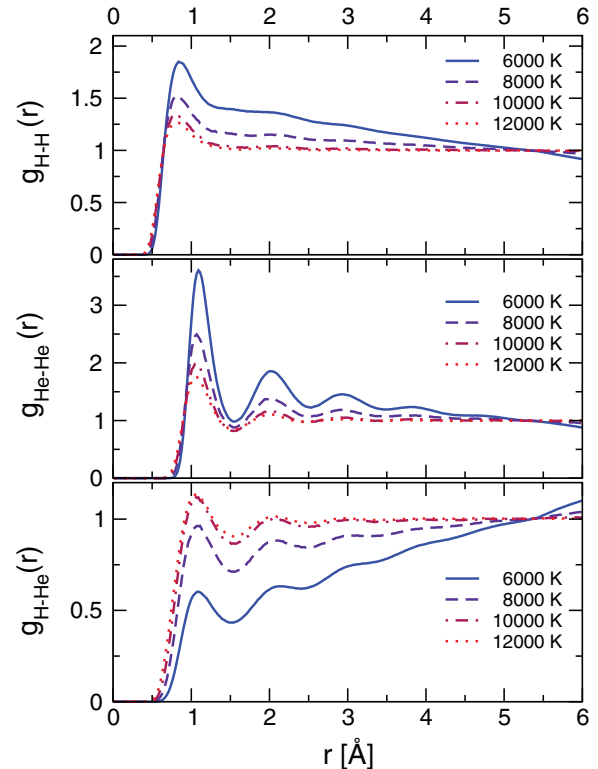

FIG. 7. (Color online) Radial distribution functions for H-H, He-He, and H-He at $\varrho = 4$ g/cm^3 and temperatures between 6000 and 12 000 K.

With increasing temperature the helium fraction inside this droplet decreases, and at 12 000 K the droplet is nearly vanished, in agreement with the results for the miscibility gap as derived from thermodynamic constraints.[22] However, since finite-size effects might still play a role, this direct method is at the moment not suitable to check the accuracy of the ideal entropy of mixing approximation.
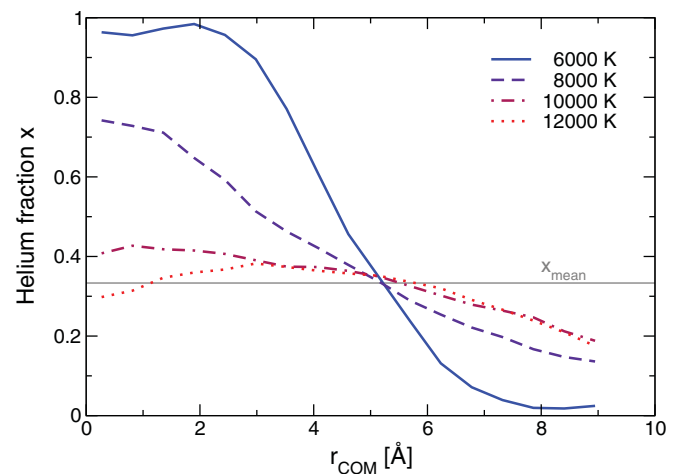

FIG. 8. (Color online) Helium fractions around the center of mass (COM) of the helium droplet for $\varrho = 4$ g/cm^3 and temperatures between 6000 and 12 000 K. The total helium fraction in the simulation box is indicated by x_{mean} (gray line).

VI. CONCLUSION

We have performed extensive calculations for the temperature-dependent electrical conductivity of hydrogen-helium mixtures at 1 and 2 Mbar, i.e., within the region where the nonmetal-to-metal transition occurs in hydrogen-rich systems. At low helium fractions the conductivity rises sharply over several orders of magnitude due to metallization in the hydrogen subsystem, while helium barely reaches metallic conductivities at the highest temperatures considered here. By extracting a temperature of metallization we show that this metallization is the driving force behind the demixing (see Fig. 4), and give revised predictions for the miscibility region in Jupiter and Saturn (Fig. 5).

By treating very large particle numbers, the phenomenon of demixing could be observed directly in the simulation box, showing the effect of demixing without any approximation for the entropy of mixing.

It would be very important to verify experimentally whether or not demixing occurs under these extreme conditions. Attempts have been made to reach the relevant parameters.[73] Since direct evidence of demixing is rather complex experimentally, a practical precursor would be very helpful. For instance, a characteristic change of the frequency-dependent reflectivity upon demixing has been predicted,[74] which could serve as a criterion for demixing. Another possibility would be to perform elastic x-ray scattering experiments on warm dense hydrogen-helium targets.[75]

[1] T. Guillot, Science **286**, 72 (1999).

[2] N. Nettelmann, B. Holst, A. Kietzmann, M. French, R. Redmer, and D. Blaschke, Astrophys. J. **683**, 1217 (2008).

[3] J. J. Fortney and N. Nettelmann, Space Sci. Rev. **152**, 423 (2010).

[4] J. J. Fortney and W. B. Hubbard, Icarus **164**, 228 (2003).

[5] J. J. Fortney and W. B. Hubbard, Astrophys. J. **608**, 1039 (2004).

[6] P. Loubeyre, R. Le Toullec, and J. P. Pinceaux, Phys. Rev. B **36**, 3723 (1987).

[7] J. A. Schouten, Int. J. Thermophys. **10**, 1 (1989).

[8] Y. J. Gu, Q. F. Chen, L. C. Cai, Z. Y. Chen, J. Zheng, and F. Q. Jing, J. Chem. Phys. **130**, 184506 (2009).

[9] V. Ternovoi, S. Kvitov, A. Pyalling, A. Filimonov, and V. Fortov, JETP Lett. **79**, 6 (2004).

[10] E. E. Salpeter, Astrophys. J. **181**, L83 (1973).

[11] D. J. Stevenson, Phys. Rev. B **12**, 3999 (1975).

[12] D. J. Stevenson and E. E. Salpeter, Astrophys. J. Suppl. Ser. **35**, 221 (1977).

[13] D. J. Stevenson and E. E. Salpeter, Astrophys. J. Suppl. Ser. **35**, 239 (1977).

[14] W. B. Hubbard and H. E. DeWitt, Astrophys. J. **290**, 388 (1985).

[15] M. S. Marley and W. B. Hubbard, Icarus **73**, 536 (1988).

[16] M. Schlanges, M. Bonitz, and A. Tschttschjan, Contrib. Plasma Phys. **35**, 109 (1995).

[17] B. Militzer, J. Low Temp. Phys. **139**, 739 (2005).

[18] J. Vorberger, I. Tamblyn, B. Militzer, and S. A. Bonev, Phys. Rev. B **75**, 024206 (2007).

[19] J. E. Klepeis, K. J. Schafer, T. W. Barbee, and M. Ross, Science **254**, 986 (1991).

[20] O. Pfaffenzeller, D. Hohl, and P. Ballone, Phys. Rev. Lett. **74**, 2599 (1995).

[21] M. A. Morales, E. Schwegler, D. Ceperley, C. Pierleoni, S. Hamel, and K. Caspersen, Proc. Natl. Acad. Sci. USA **106**, 1324 (2009).

[22] W. Lorenzen, B. Holst, and R. Redmer, Phys. Rev. Lett. **102**, 115701 (2009).

[23] L. Landau and J. Zeldovich, Acta Physicochim. URSS **18**, 194 (1943).

[24] S. T. Weir, A. C. Mitchell, and W. J. Nellis, Phys. Rev. Lett. **76**, 1860 (1996).

[25] W. J. Nellis, S. T. Weir, and A. C. Mitchell, Phys. Rev. B **59**, 3434 (1999).

[26] V. E. Fortov, R. I. Ilkaev, V. A. Arinin, V. V. Burtzev, V. A. Golubev, I. L. Iosilevskiy, V. V. Khrustalev, A. L. Mikhailov, M. A. Mochalov, V. Y. Ternovoi, and M. V. Zhernokletov, Phys. Rev. Lett. **99**, 185001 (2007).

[27] W. Ebeling and W. Richert, Phys. Lett. A **108**, 80 (1985).

[28] D. Saumon and G. Chabrier, Phys. Rev. Lett. **62**, 2397 (1989).

[29] H. Reinholz, R. Redmer, and S. Nagel, Phys. Rev. E **52**, 5368 (1995).

[30] D. Beule, W. Ebeling, A. Förster, H. Juranek, S. Nagel, R. Redmer, and G. Röpke, Phys. Rev. B **59**, 14177 (1999).

[31] B. Holst, N. Nettelmann, and R. Redmer, Contrib. Plasma Phys. **47**, 368 (2007).

[32] M. A. Morales, C. Pierleoni, E. Schwegler, and D. M. Ceperley, Proc. Natl. Acad. Sci. USA **107**, 12799 (2010).

[33] W. Lorenzen, B. Holst, and R. Redmer, Phys. Rev. B **82**, 195107 (2010).

[34] G. Kresse and J. Hafner, Phys. Rev. B **47**, 558 (1993).

[35] G. Kresse and J. Hafner, Phys. Rev. B **49**, 14251 (1994).

[36] G. Kresse and J. Furthmüller, Phys. Rev. B **54**, 11169 (1996).

[37] P. Hohenberg and W. Kohn, Phys. Rev. **136**, B864 (1964).

[38] W. Kohn and L. J. Sham, Phys. Rev. **140**, A1133 (1965).

[39] N. D. Mermin, Phys. Rev. **137**, A1441 (1965).

[40] A. Kietzmann, B. Holst, R. Redmer, M. P. Desjarlais, and T. R. Mattsson, Phys. Rev. Lett. **98**, 190602 (2007).

[41] B. Holst, R. Redmer, and M. P. Desjarlais, Phys. Rev. B **77**, 184201 (2008).

[42] L. Caillabet, S. Mazevet, and P. Loubeyre, Phys. Rev. B **83**, 094101 (2011).

[43]P. E. Blöchl, Phys. Rev. B **50**, 17953 (1994).

[44]G. Kresse and D. Joubert, Phys. Rev. B **59**, 1758 (1999).

[45]J. P. Perdew, K. Burke, and M. Ernzerhof, Phys. Rev. Lett. **77**, 3865 (1996).

[46]A. Baldereschi, Phys. Rev. B **7**, 5212 (1973).

[47]S. Nosé, J. Chem. Phys. **81**, 511 (1984).

[48]R. Kubo, J. Phys. Soc. Jpn. **12**, 570 (1957).

[49]D. A. Greenwood, Proc. Phys. Soc. London **71**, 585 (1958).

[50]M. P. Desjarlais, J. D. Kress, and L. A. Collins, Phys. Rev. E **66**, 025401(R) (2002).

[51]S. Mazevet, M. Torrent, V. Recoules, and F. Jollet, High Energy Density Phys. **6**, 84 (2010).

[52]B. Holst, M. French, and R. Redmer, Phys. Rev. B **83**, 235120 (2011).

[53]H. J. Monkhorst and J. D. Pack, Phys. Rev. B **13**, 5188 (1976).

[54]P. P. Edwards, M. T. J. Lodge, F. Hensel, and R. Redmer, Philos. Trans. R. Soc. A **368**, 941 (2010).

[55]P. M. Kowalski, S. Mazevet, D. Saumon, and M. Challacombe, Phys. Rev. B **76**, 075112 (2007).

[56]L. Stixrude and R. Jeanloz, Proc. Natl. Acad. Sci. USA **32**, 11071 (2008).

[57]B. Militzer, Phys. Rev. B **79**, 155105 (2009).

[58]I. Tamblyn and S. A. Bonev, Phys. Rev. Lett. **104**, 065702 (2010).

[59]M. Städele and R. M. Martin, Phys. Rev. Lett. **84**, 6070 (2000).

[60]J. Heyd, G. E. Scuseria, and M. Ernzerhof, J. Chem. Phys. **118**, 8207 (2003).

[61]M. French, T. R. Mattsson, and R. Redmer, Phys. Rev. B **82**, 174108 (2010).

[62]K. A. Johnson and N. W. Ashcroft, Phys. Rev. B **58**, 15548 (1998).

[63]B. Militzer, Phys. Rev. Lett. **97**, 175501 (2006).

[64]M. A. Morales, C. Pierleoni, and D. M. Ceperley, Phys. Rev. E **81**, 021202 (2010).

[65]V. V. Kechin, J. Phys. Condens. Matter **7**, 531 (1995).

[66]R. K. Crawford and W. B. Daniels, J. Chem. Phys. **55**, 5651 (1971).

[67]R. L. Mills, D. H. Liebenberg, and J. C. Bronson, Phys. Rev. B **21**, 5137 (1980).

[68]W. L. Vos, M. G. E. van Hinsberg, and J. A. Schouten, Phys. Rev. B **42**, 6106 (1990).

[69]F. Datchi, P. Loubeyre, and R. Le Toullec, Phys. Rev. B **61**, 6535 (2000).

[70]D. Santamaría-Pérez, G. D. Mukherjee, B. Schwager, and R. Boehler, Phys. Rev. B **81**, 214101 (2010).

[71]J. A. Schouten, A. de Kuijper, and J. P. J. Michels, Phys. Rev. B **44**, 6630 (1991).

[72]W. Humphrey, A. Dalke, and K. Schulten, J. Mol. Graphics **14**, 33 (1996).

[73]P. Loubeyre (private communication).

[74]S. Hamel, M. A. Morales, and E. Schwegler, Phys. Rev. B **84**, 165110 (2011).

[75]K. Wünsch, J. Vorberger, G. Gregori, and D. O. Gericke, Europhys. Lett. **94**, 25001 (2011).